Bayesian Compressive Sensing Failure Detection in Planar Phased Antenna Arrays

M. Salucci, A. Gelmini, G. Oliveri, and A. Massa

Abstract

The diagnosis of planar phased antenna arrays is dealt with in this work. The retrieval of the faulty radiators in the antenna under test (*AUT*) is formulated within the compressive sensing (*CS*) framework and it is efficiently and effectively solved through a customized Bayesian *CS* (*BCS*) solver. Robust and reliable reconstructions of the *AUT* status are yielded by means of the proposed diagnosis tool also in presence of significant amounts of noise on processed far-field data. Some numerical experiments are presented to assess the *BCS*-based method when dealing with different operative conditions as well as considering a variation of the array size and failure rate.

Contents

1 Numerical Validation

1.1 Taylor Array, $N = 716$, Isotropic Sources

Parameters

- Gold Array
  - Total number of elements: $N = 716$;
  - Type of elements: isotropic/ideal [1];
  - Spacing along x and y: $d_x = d_y = 0.5$ [λ];
  - Excitation tapering: Taylor;
    - Radius: $R = 7.5$ [λ];
    - Transition index: $t = 3$;
    - Peak sidelobe level: $PSL = 25$ [dB];

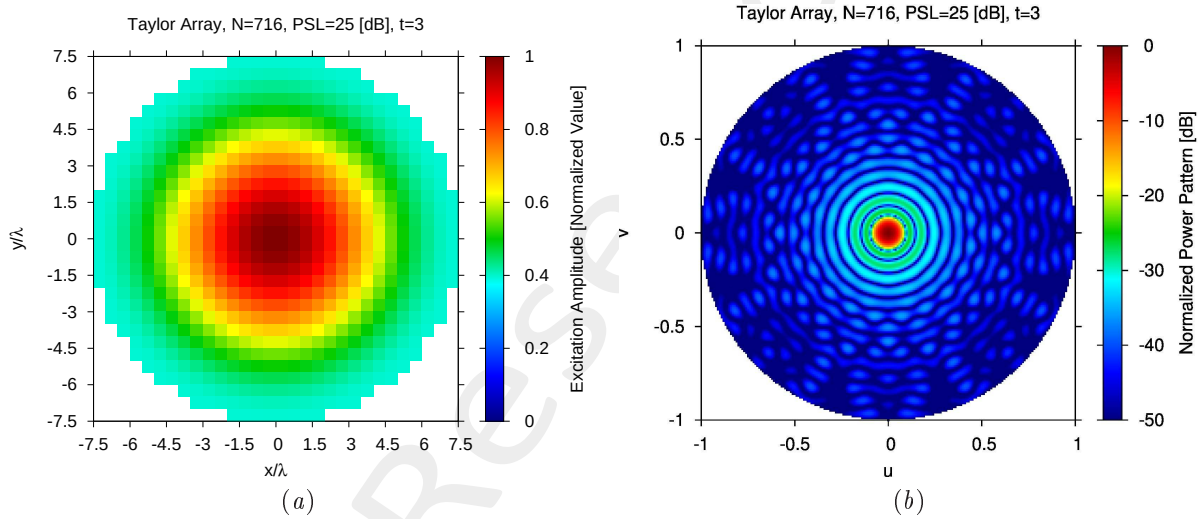

Figure 1: (a) Array excitations and (b) normalized power pattern of the expected array (gold antenna).

- Failed Array
  - Failure factor: $\kappa = 0$ (total failures);
  - Failure rate: see table below;

N_f	$\Phi = \frac{N_f}{N}$
7	1%
14	2%
29	4%
57	8%
115	16%

Table 1: Number of failures (N_f) and corresponding failure rate ($\Phi = \frac{N_f}{N}$).

[1] In order to model *isotropic* radiators, let us assume that the embedded elements patterns are equal to $F_\theta^{(n)}(u, v) = 1$ and $F_\varphi^{(n)}(u, v) = 0$, for $n = 1, ..., N$.

- Measurement set-up
  - Type of sampling: uniform sampling in the (u, v) plane;
  - Number of points in the visible range: $K = 317$;
  - Ratio between measurements and number of elements: $\nu = \frac{K}{N} \simeq 1.0$ $(\nu^{(opt)})$;
- *BCS* solver
  - Noise variance: $\eta = 5 \times 10^{-1}$ $(\eta^{(opt)})$;
  - Tolerance factor: $\iota = 10^{-8}$;
- Signal-to-Noise-Ratio: $SNR = \{10; 20; ...; 100\}$.

Results

$\Phi = \frac{N_f}{N} = 1\%$ $(N_f = 7)$ - **Best and Worst** BCS **Reconstructions**

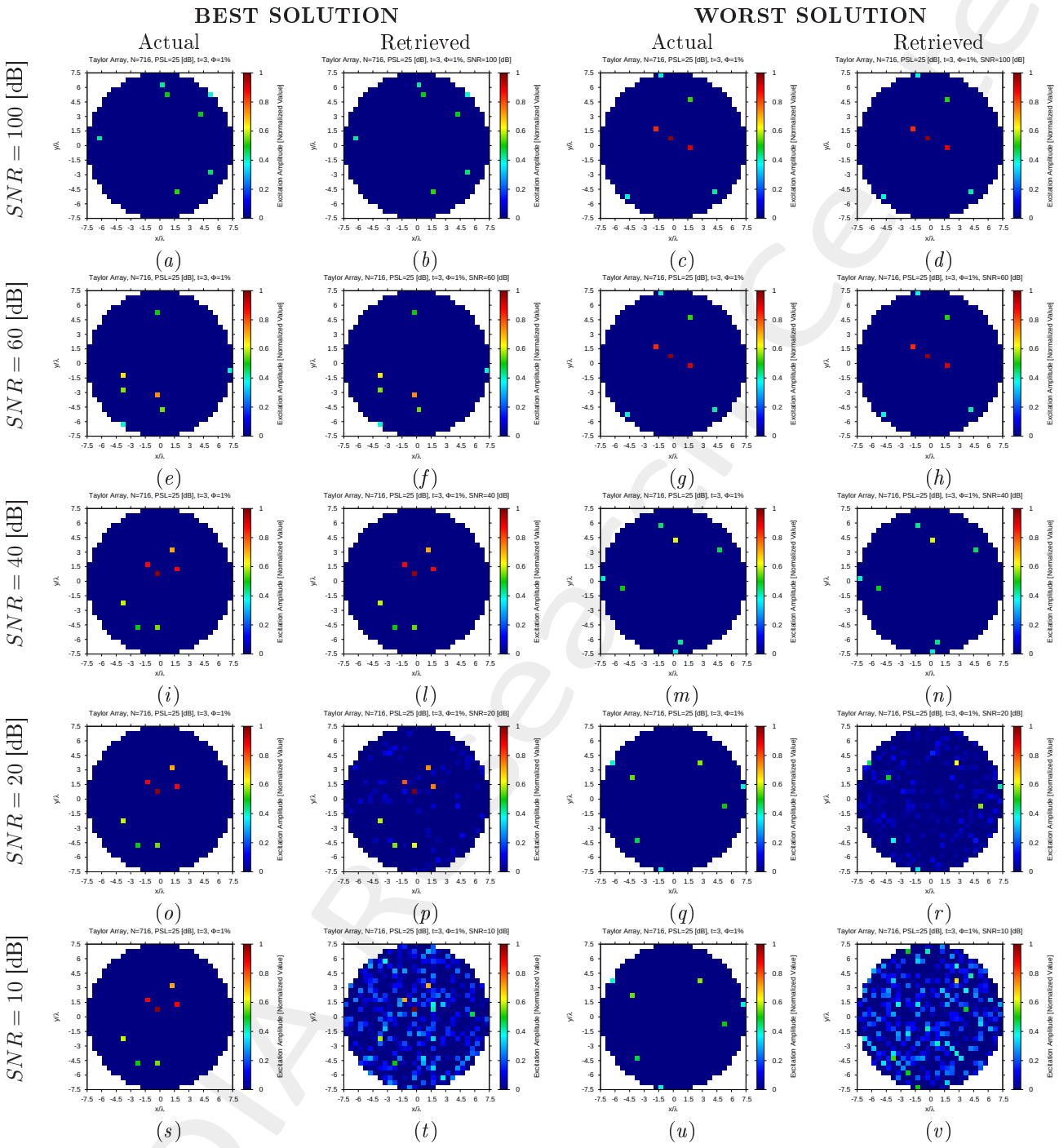

Figure 2: Taylor Array ($N = 716$, $PSL = 25$ [dB], $t = 3$, $\Phi = 1\%$) - Best and worst reconstructions by BCS under several SNR values.

$\Phi = \frac{N_f}{N} = 2\%$ $(N_f = 14)$ - **Best and Worst** BCS **Reconstructions**

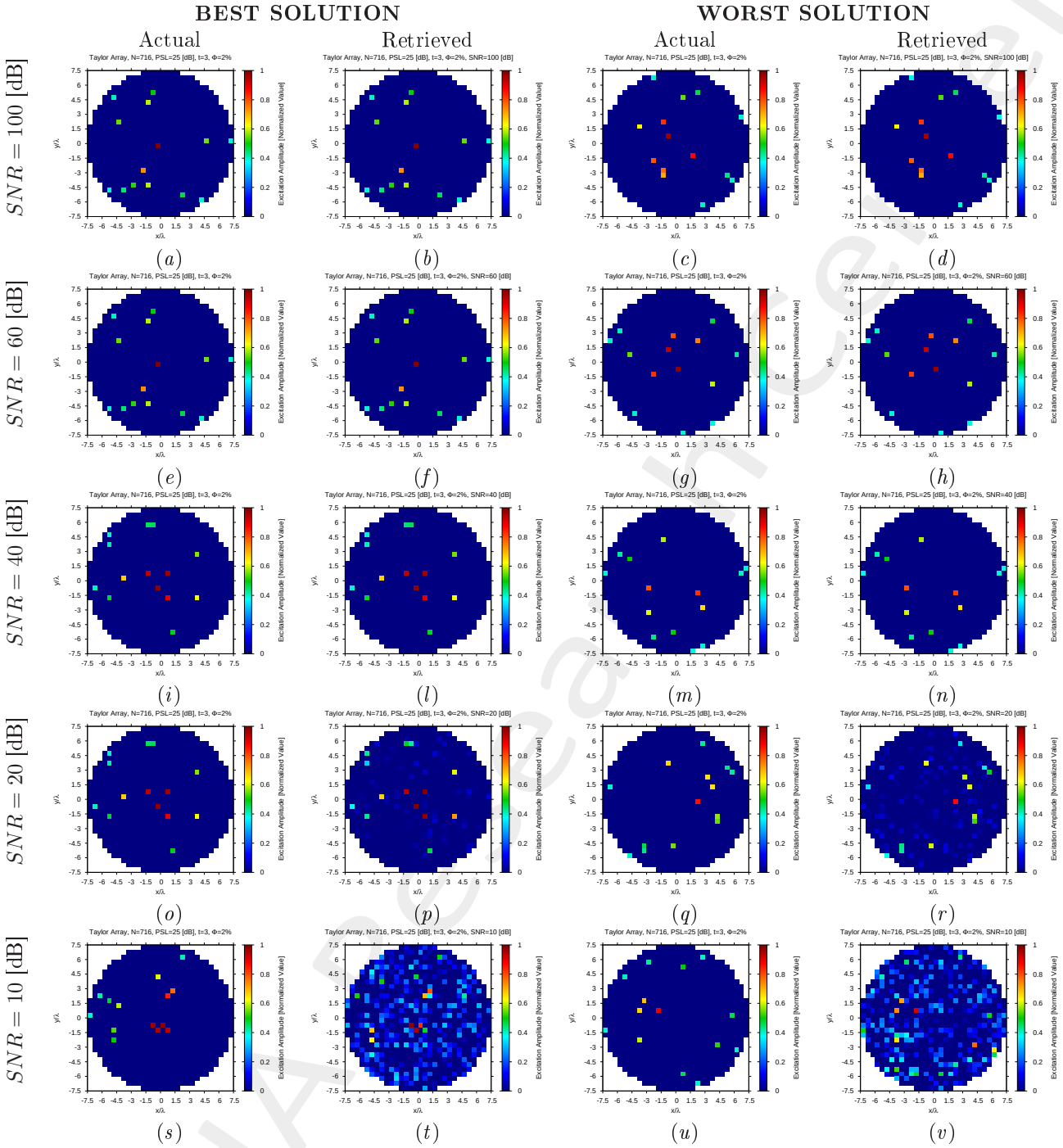

Figure 3: Taylor Array ($N = 716$, $PSL = 25$ [dB], $t = 3$, $\Phi = 2\%$) - Best and worst reconstructions by BCS under several SNR values.

$\Phi = \frac{N_f}{N} = 4\%$ ($N_f = 29$) - **Best and Worst** BCS **Reconstructions**

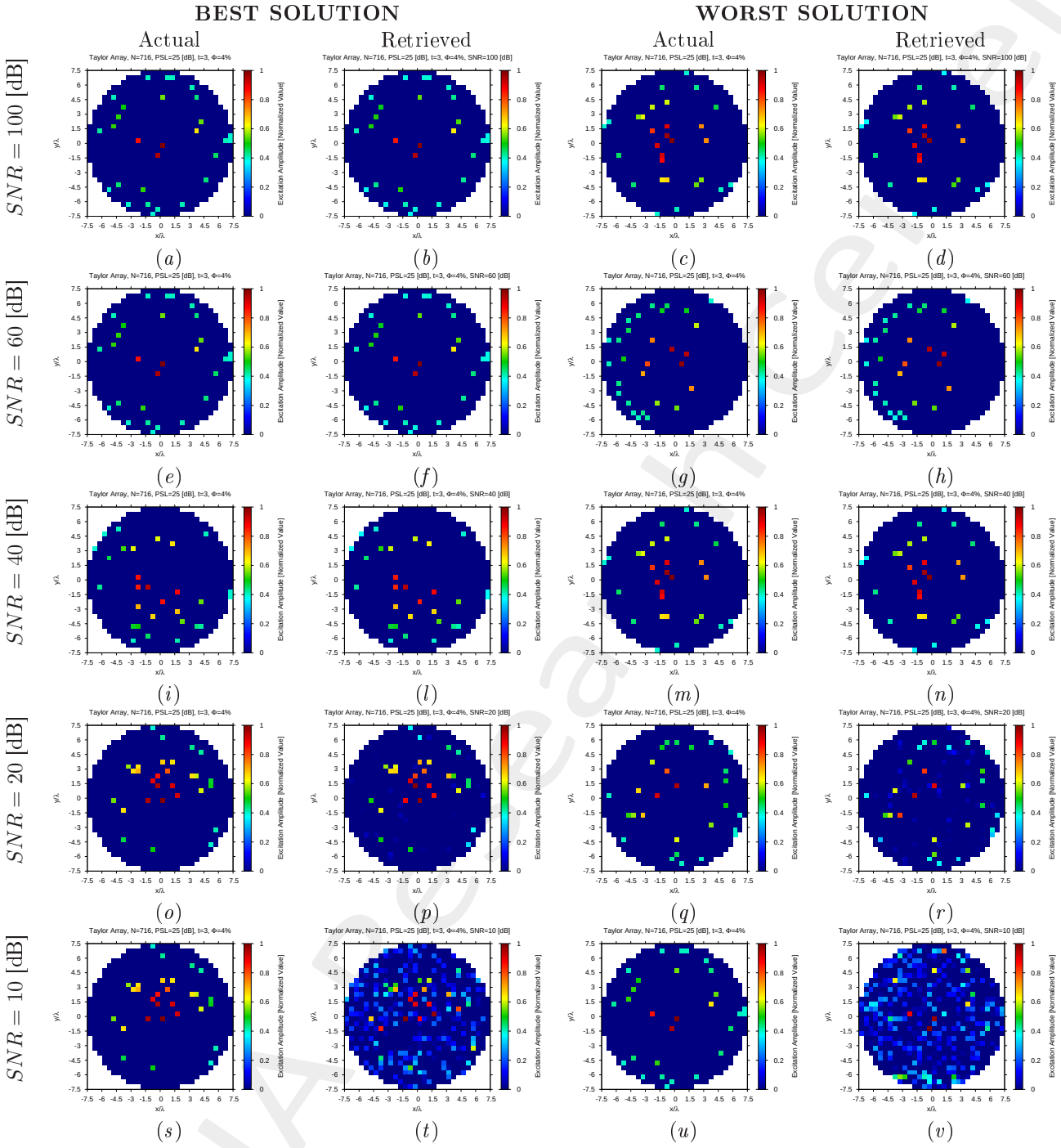

Figure 4: Taylor Array ($N = 716$, $PSL = 25$ [dB], $t = 3$, $\Phi = 4\%$) - Best and worst reconstructions by BCS under several SNR values.

$\Phi = \frac{N_f}{N} = 8\%$ $(N_f = 57)$ - **Best and Worst** BCS **Reconstructions**

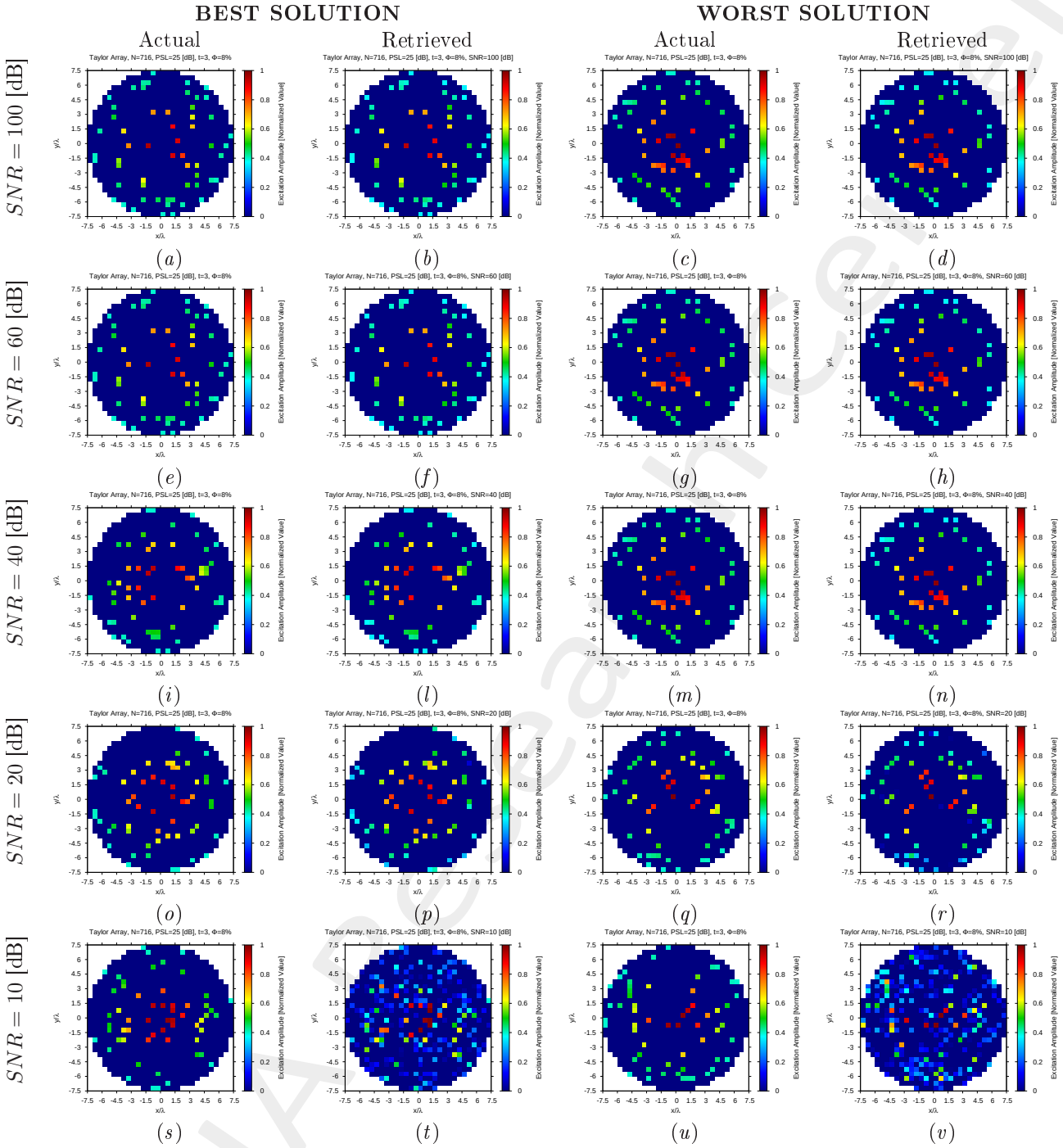

Figure 5: Taylor Array ($N = 716$, $PSL = 25$ [dB], $t = 3$, $\Phi = 8\%$) - Best and worst reconstructions by BCS under several SNR values.

$\Phi = \frac{N_f}{N} = 16\%$ $(N_f = 115)$ - **Best and Worst** BCS **Reconstructions**

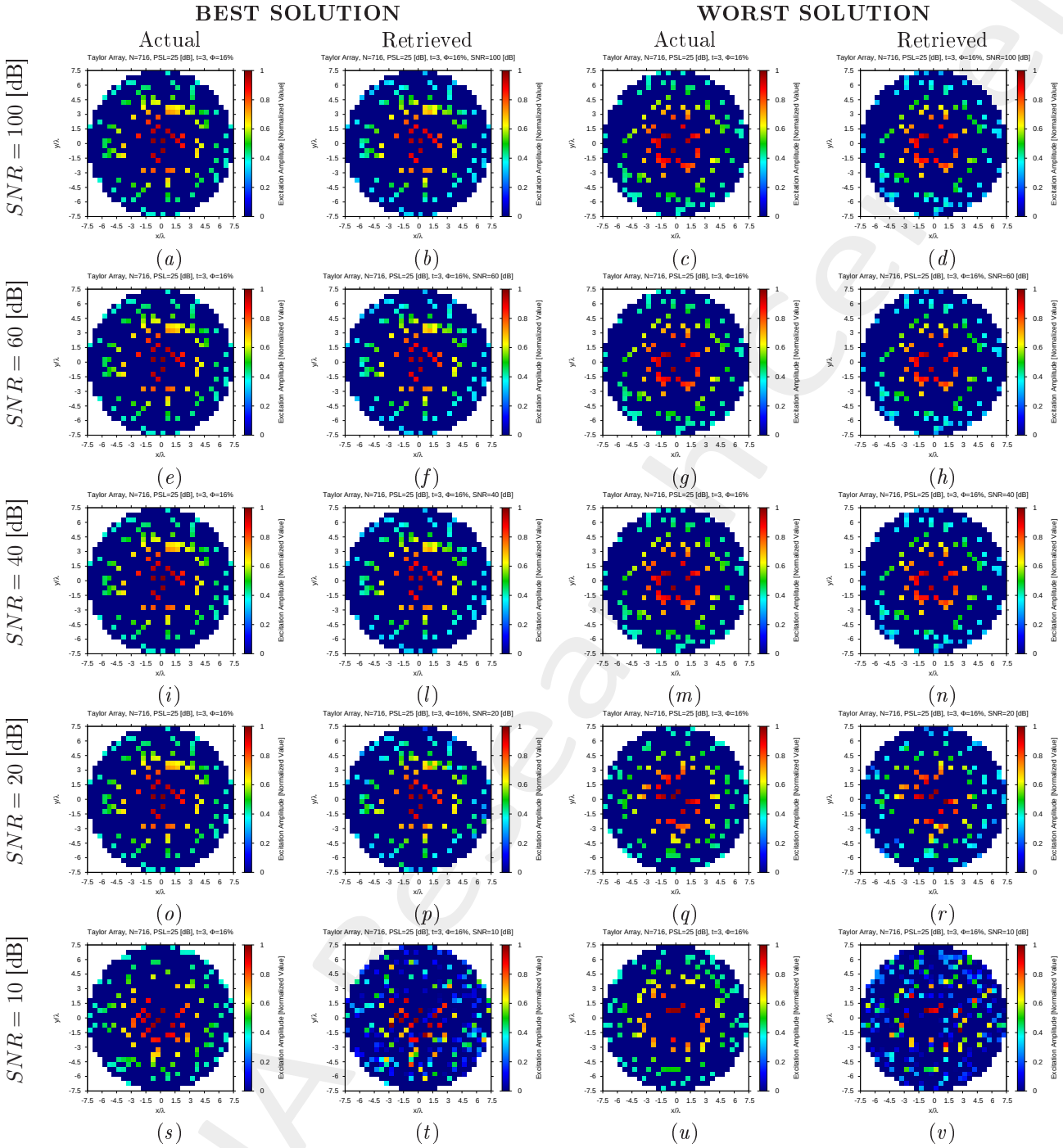

Figure 6: Taylor Array ($N = 716$, $PSL = 25$ [dB], $t = 3$, $\Phi = 16\%$) - Best and worst reconstructions by BCS under several SNR values.

Diagnosis Error and Confidence Level

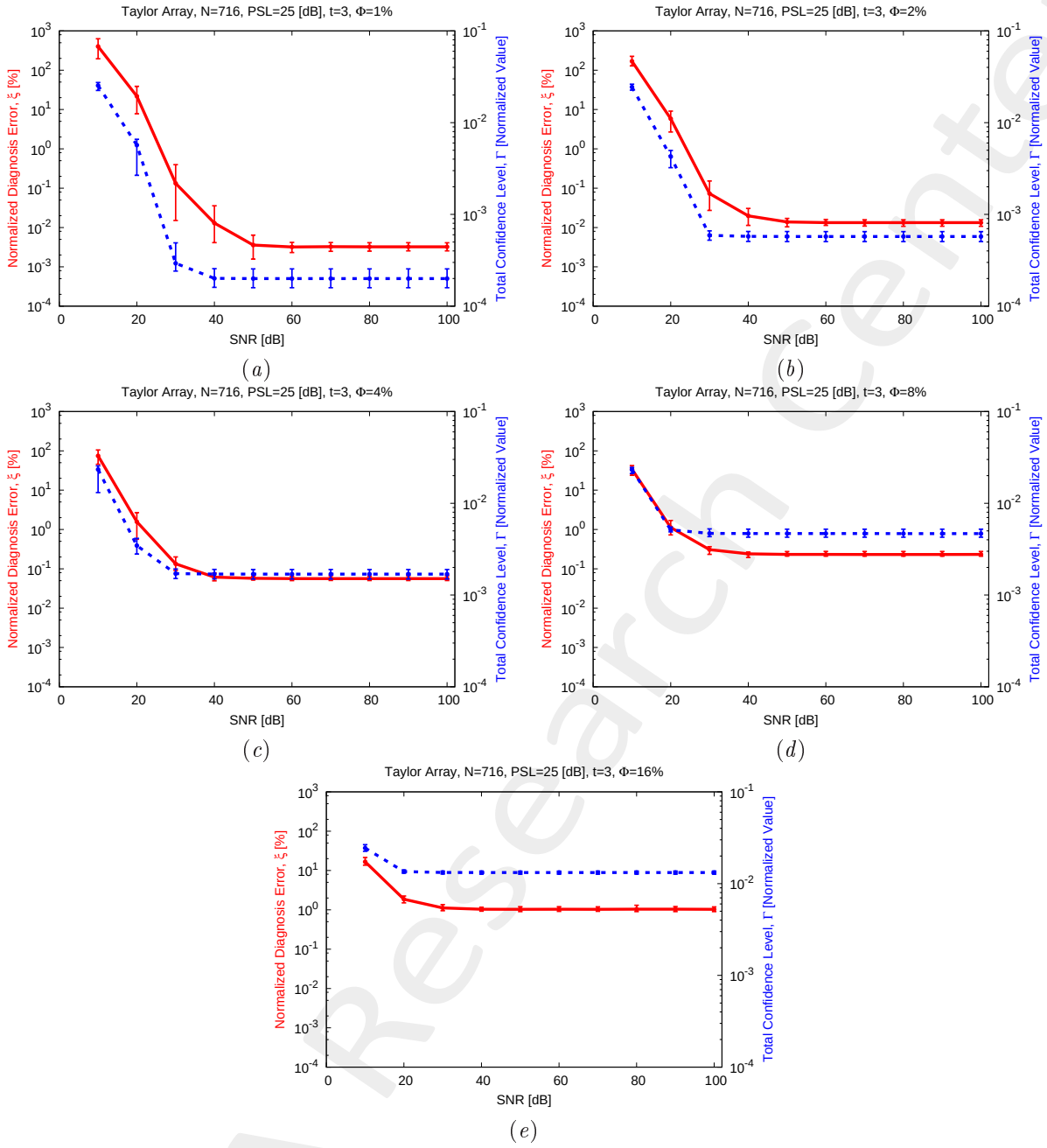

Figure 7: Taylor Array ($N = 716$, $PSL = 25$ [dB], $t = 3$) - Behavior of the average, minimum and maximum diagnosis error (ξ) and total confidence level (Γ) versus the SNR, for (a) $\Phi = 1\%$, (b) $\Phi = 2\%$, (c) $\Phi = 4\%$, (d) $\Phi = 8\%$, and (e) $\Phi = 16\%$.

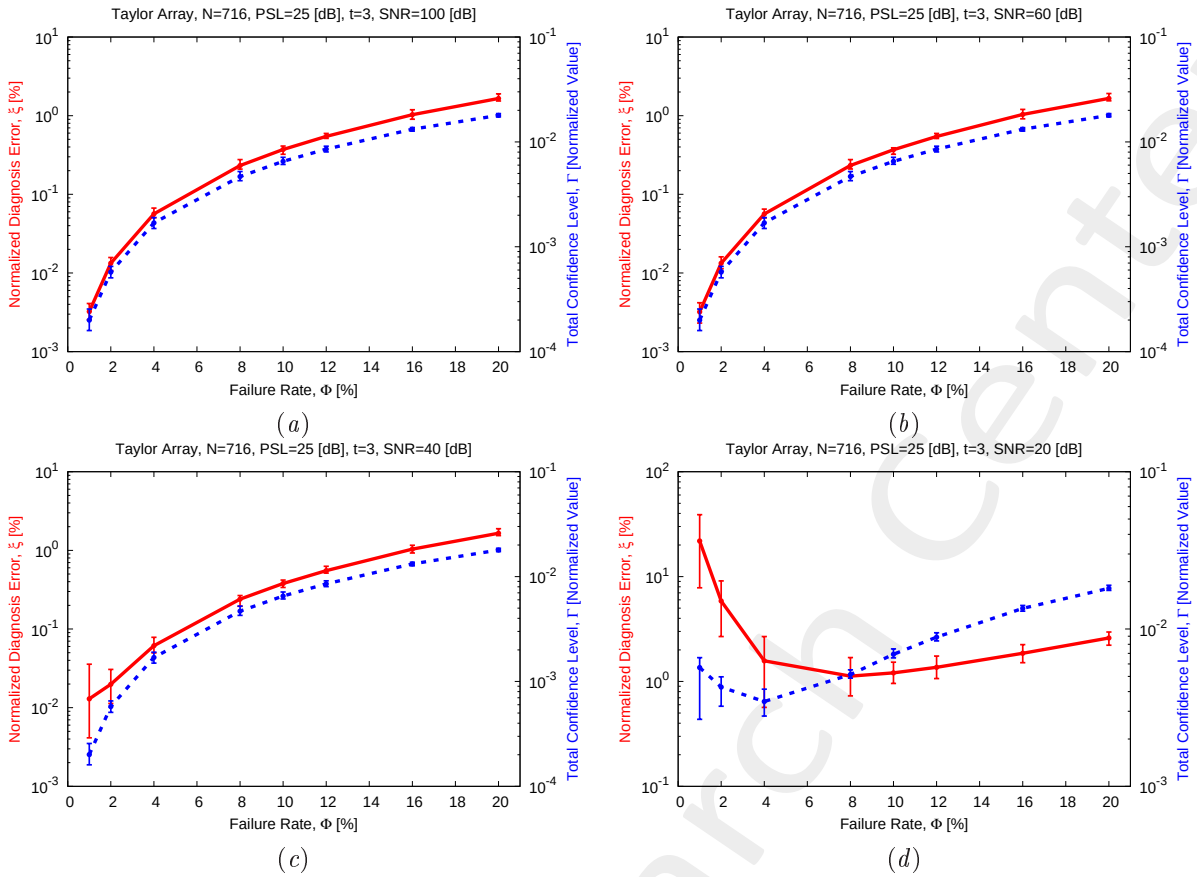

Figure 8: Taylor Array ($N = 716$, $PSL = 25$ [dB], $t = 3$) - Behavior of the average, minimum and maximum diagnosis error (ξ) and total confidence level (Γ) versus the failure rate (Φ), for (a) $SNR = 100$ [dB], (b) $SNR = 60$ [dB], (c) $SNR = 40$ [dB], and (d) $SNR = 20$ [dB].

1.2 Taylor Array, $N = 1264$, Isotropic Sources

Parameters

- Gold Array
  - Total number of elements: $N = 1264$;
  - Type of elements: isotropic/ideal [2];
  - Spacing along x and y: $d_x = d_y = 0.5$ [λ];
  - Excitation tapering: Taylor;
    - Radius: $R = 9.75$ [λ];
    - Transition index: $t = 3$;
    - Peak sidelobe level: $PSL = 25$ [dB]

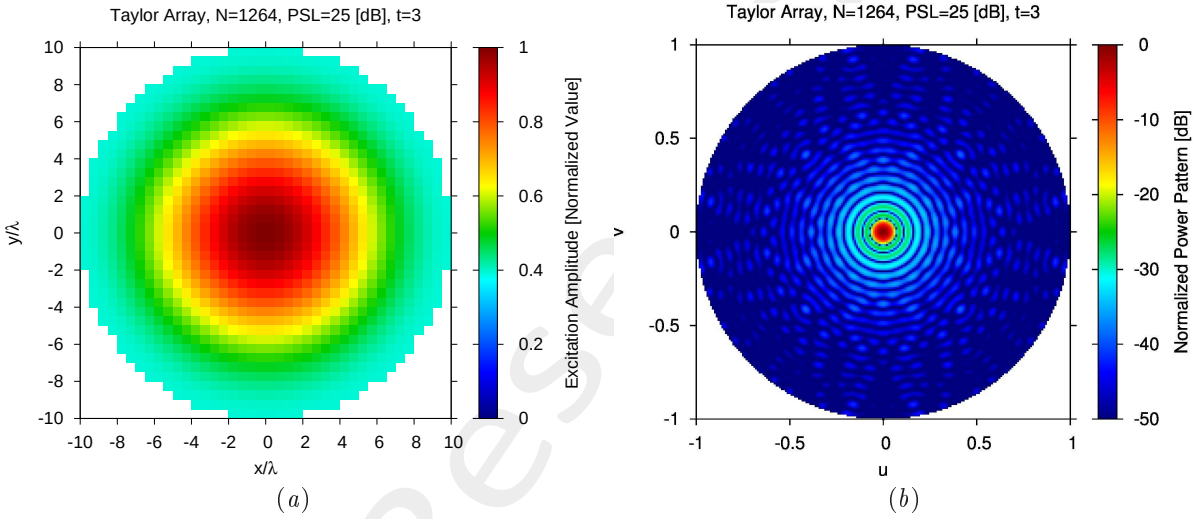

Figure 9: (a) Array excitations and (b) normalized power pattern of the expected array (gold antenna).

- Failed Array
  - Failure factor: $\kappa = 0$;
  - Failure rate: see table below;

N_f	$\Phi = \frac{N_f}{N}$
13	1%
25	2%
51	4%
101	8%
202	16%

Table 2: Number of failures (N_f) and corresponding failure rate ($\Phi = \frac{N_f}{N}$).

[2] In order to model *isotropic* radiators, let us assume that the embedded elements patterns are equal to $F_\theta^{(n)}(u, v) = 1$ and $F_\varphi^{(n)}(u, v) = 0$, for $n = 1, ..., N$.

- Measurement set-up
  - Type of sampling: uniform sampling in the (u, v) plane;
  - Number of points in the visible range: $K = 1257$;
  - Ratio between measurements and number of elements: $\nu = \frac{K}{N} \simeq 1.0$ $(\nu^{(opt)})$;
- BCS solver
  - Noise variance: $\eta = 5 \times 10^{-1}$ $(\eta^{(opt)})$;
  - Tolerance factor: $\iota = 10^{-8}$;
- Signal-to-Noise-Ratio: $SNR = \{10; 20; ...; 100\}$.

Results

$\Phi = \frac{N_f}{N} = 1\%$ $(N_f = 13)$ - **Best and Worst** BCS **Reconstructions**

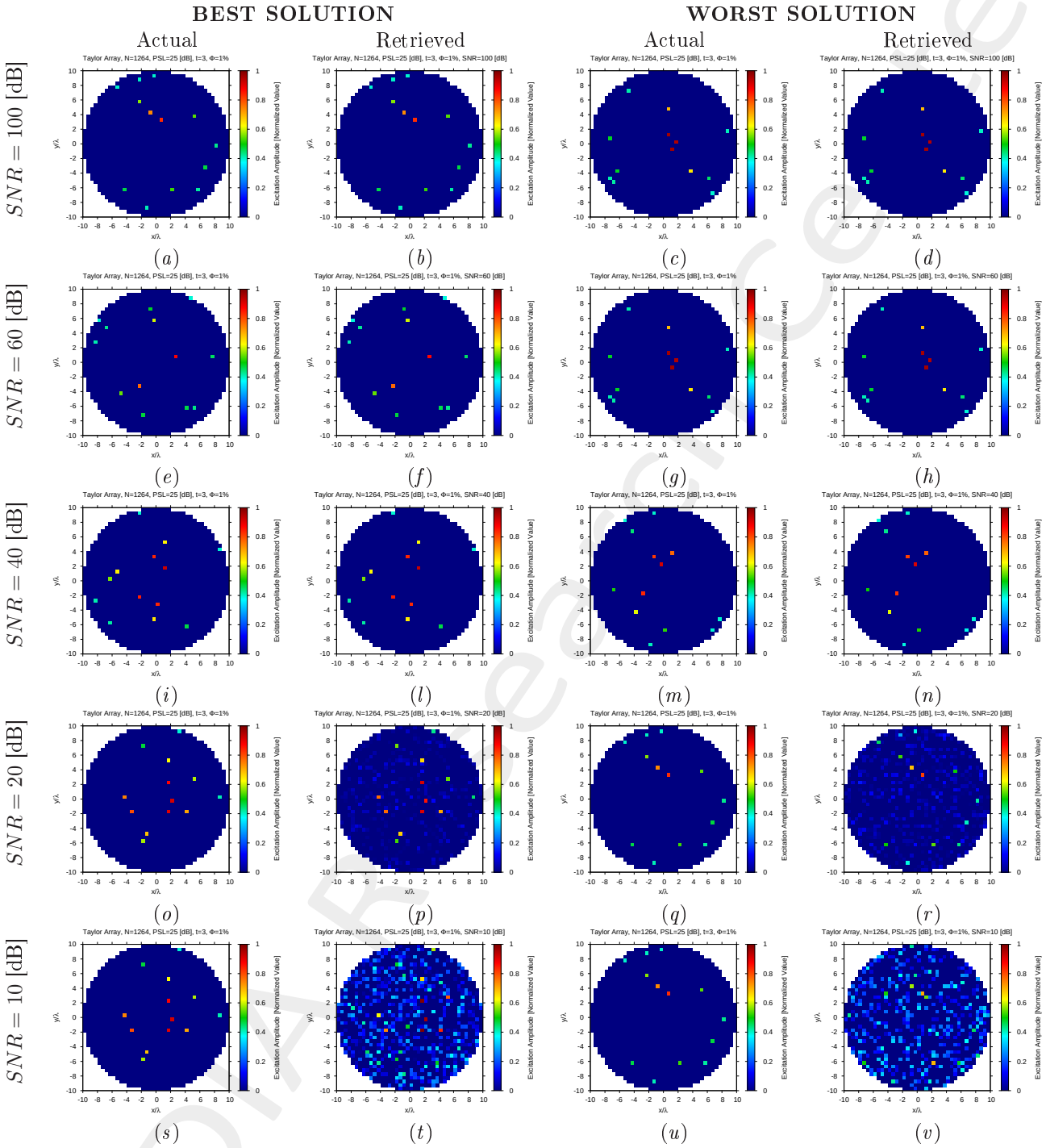

Figure 10: Taylor Array ($N = 1264$, $PSL = 25$ [dB], $t = 3$, $\Phi = 1\%$) - Best and worst reconstructions by BCS under several SNR values.

$\Phi = \frac{N_f}{N} = 2\%$ ($N_f = 25$) - **Best and Worst** BCS **Reconstructions**

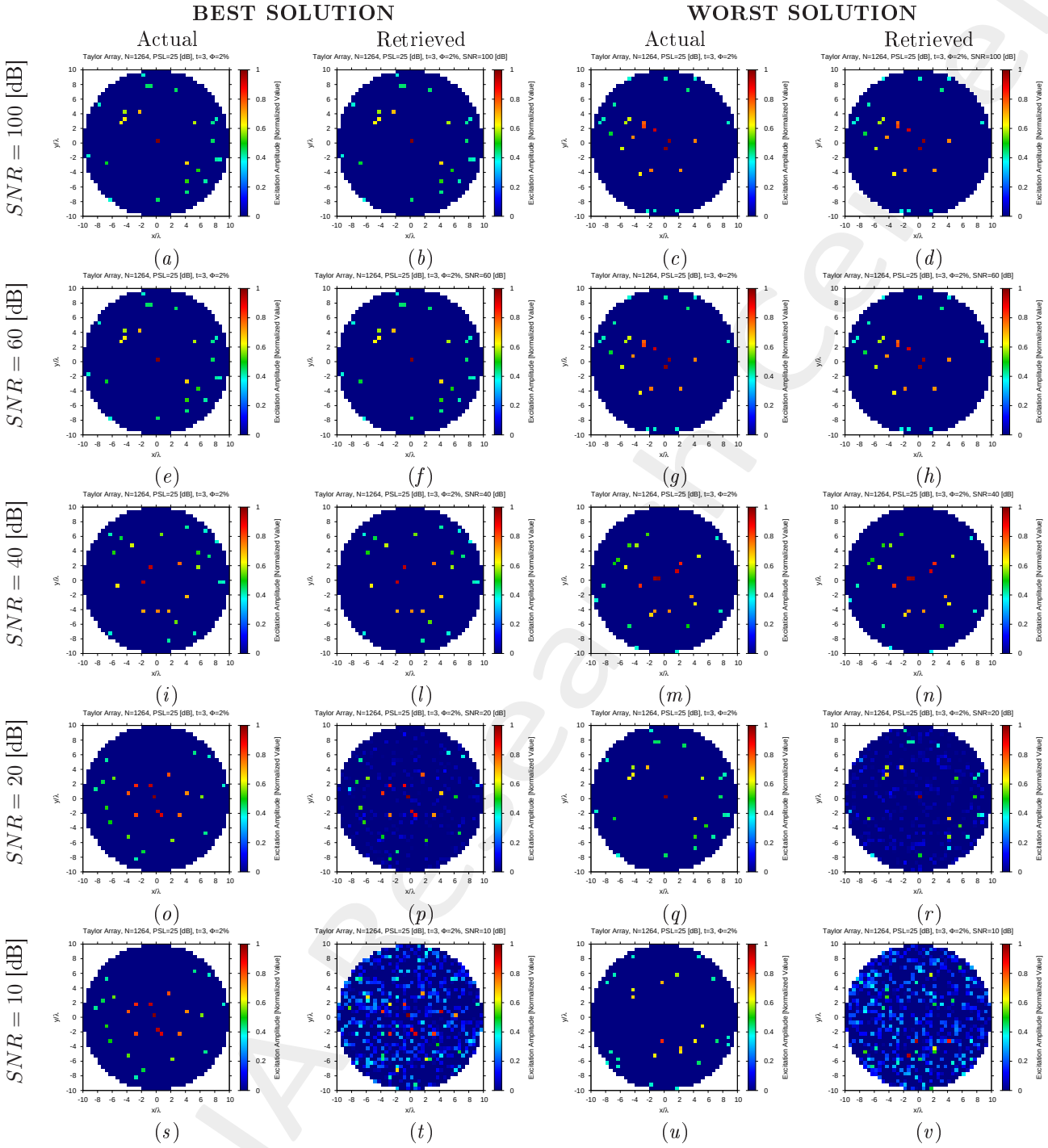

Figure 11: Taylor Array ($N = 1264$, $PSL = 25$ [dB], $t = 3$, $\Phi = 2\%$) - Best and worst reconstructions by BCS under several SNR values.

$\Phi = \frac{N_f}{N} = 4\%$ $(N_f = 51)$ - **Best and Worst** BCS **Reconstructions**

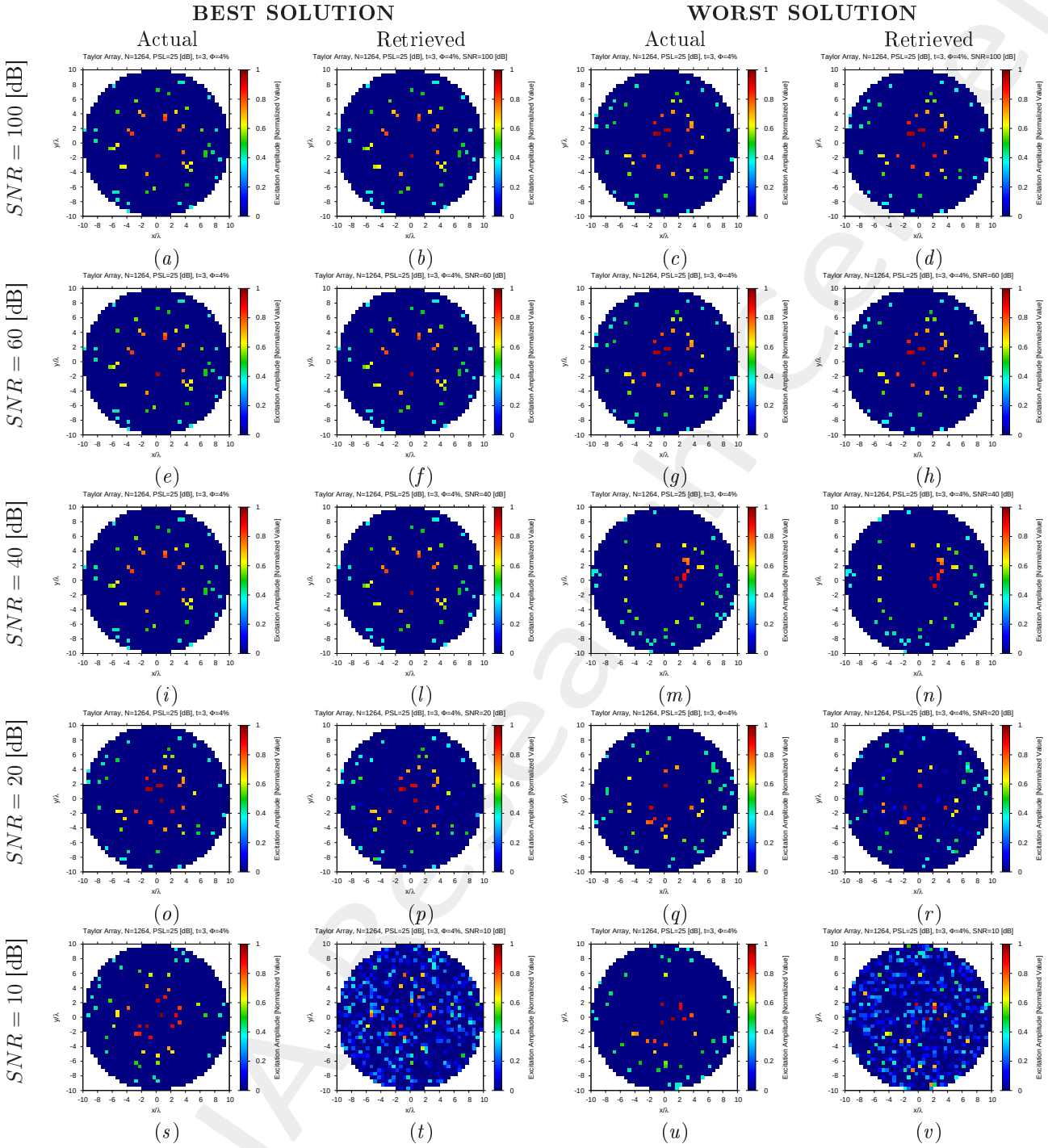

Figure 12: Taylor Array ($N = 1264$, $PSL = 25$ [dB], $t = 3$, $\Phi = 4\%$) - Best and worst reconstructions by BCS under several SNR values.

$\Phi = \frac{N_f}{N} = 8\%$ $(N_f = 101)$ - **Best and Worst** BCS **Reconstructions**

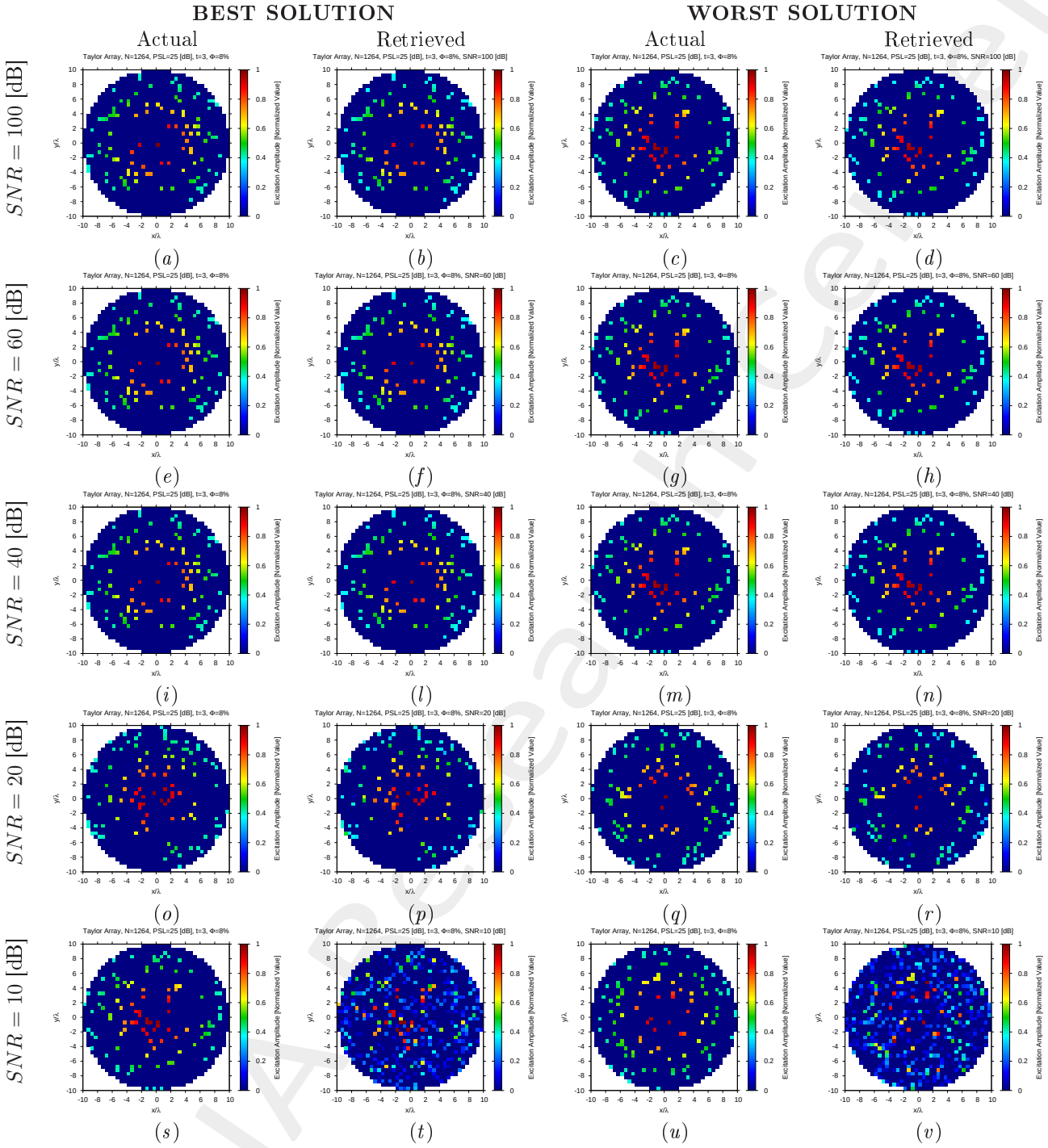

Figure 13: Taylor Array ($N = 1264$, $PSL = 25$ [dB], $t = 3$, $\Phi = 8\%$) - Best and worst reconstructions by BCS under several SNR values.

$\Phi = \frac{N_f}{N} = 16\%$ $(N_f = 202)$ - **Best and Worst** BCS **Reconstructions**

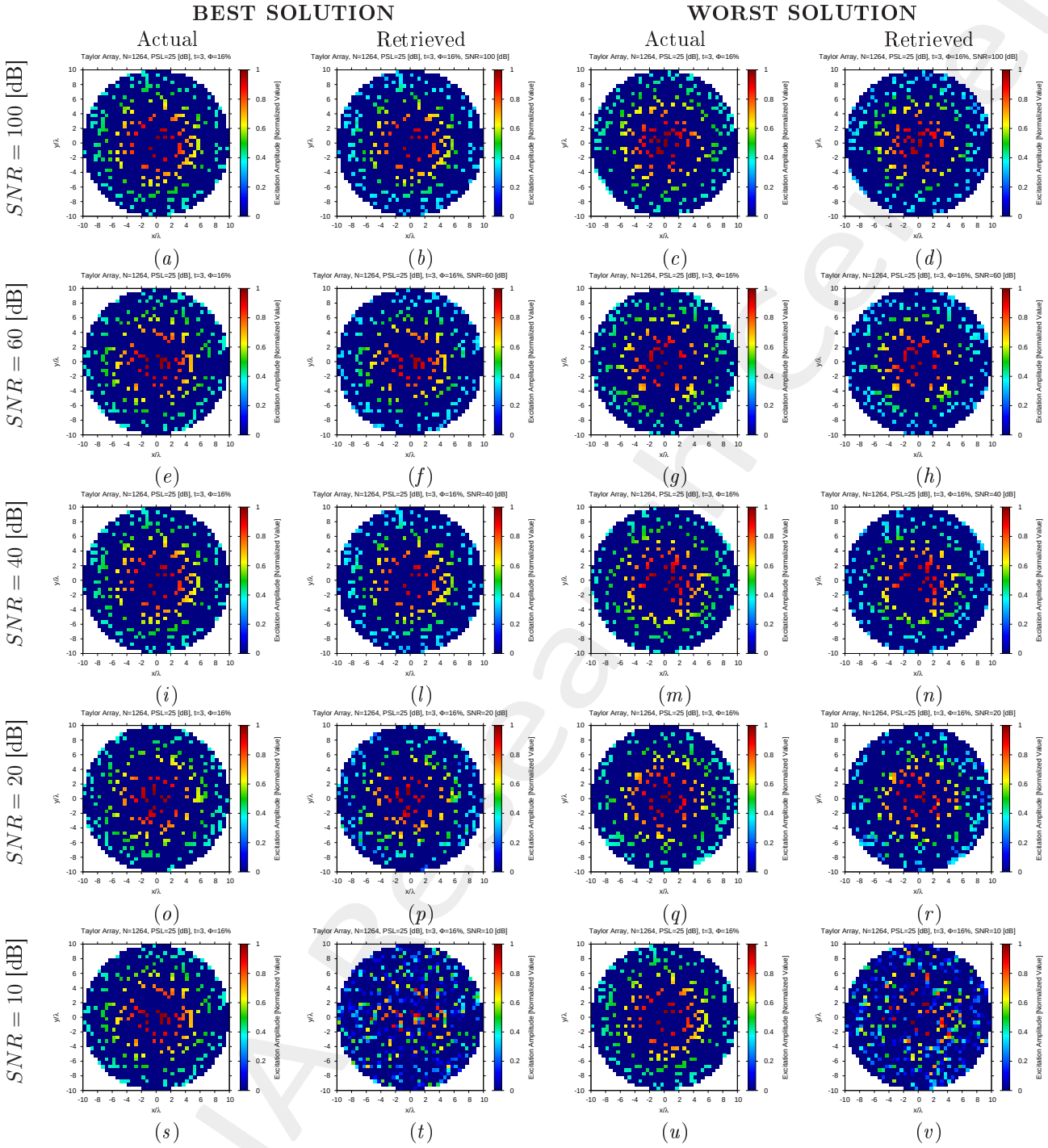

Figure 14: Taylor Array ($N = 1264$, $PSL = 25$ [dB], $t = 3$, $\Phi = 16\%$) - Best and worst reconstructions by BCS under several SNR values.

Diagnosis Error and Confidence Level

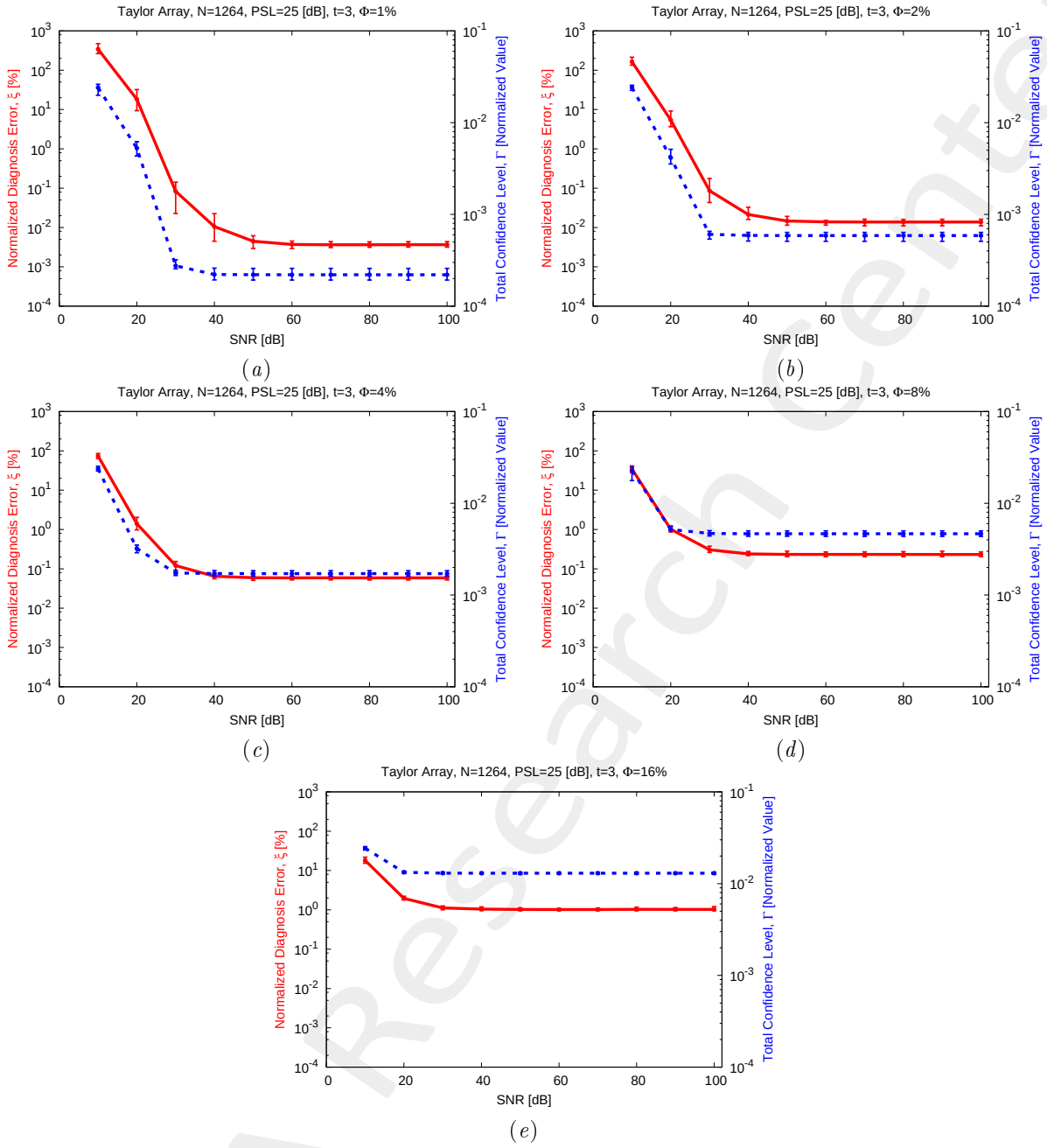

Figure 15: Taylor Array ($N = 1264$, $PSL = 25$ [dB], $t = 3$) - Behavior of the average, minimum and maximum diagnosis error (ξ) and total confidence level (Γ) versus the SNR, for (a) $\Phi = 1\%$, (b) $\Phi = 2\%$, (c) $\Phi = 4\%$, (d) $\Phi = 8\%$, and (e) $\Phi = 16\%$.

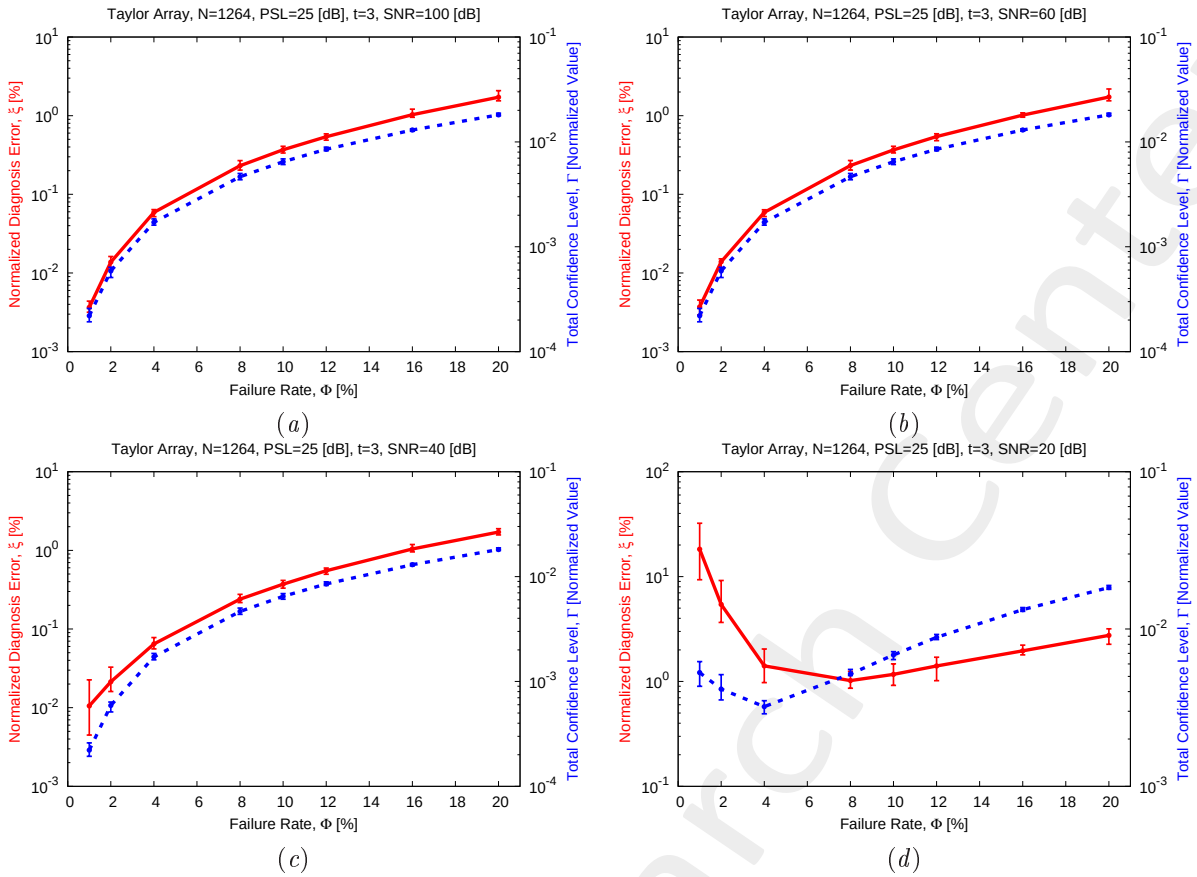

Figure 16: Taylor Array ($N = 1264$, $PSL = 25$ [dB], $t = 3$) - Behavior of the average, minimum and maximum diagnosis error (ξ) and total confidence level (Γ) versus the failure rate (Φ), for (a) $SNR = 100$ [dB], (b) $SNR = 60$ [dB], (c) $SNR = 40$ [dB], and (d) $SNR = 20$ [dB].

1.3 Taylor Array, $N = 1976$, Isotropic Sources

Parameters

- Gold Array
  - Total number of elements: $N = 1976$;
  - Type of elements: isotropic/ideal [3];
  - Spacing along x and y: $d_x = d_y = 0.5$ [λ];
  - Excitation tapering: Taylor;
    - Radius: $R = 12.5$ [λ];
    - Transition index: $t = 3$;
    - Peak sidelobe level: $PSL = 25$ [dB];

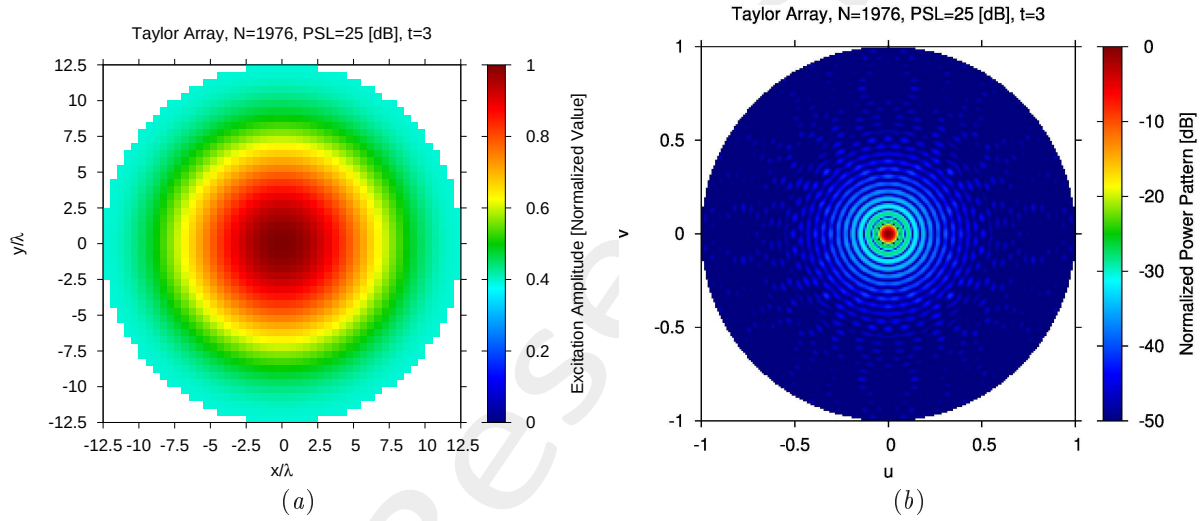

Figure 17: (a) Array excitations and (b) normalized power pattern of the expected array (gold antenna).

- Failed Array
  - Failure factor: $\kappa = 0$;
  - Failure rate: see table below;

N_f	$\Phi = \frac{N_f}{N}$
20	1%
40	2%
79	4%
158	8%
316	16%

Table 3: Number of failures (N_f) and corresponding failure rate ($\Phi = \frac{N_f}{N}$).

[3] In order to model *isotropic* radiators, let us assume that the embedded elements patterns are equal to $F_\theta^{(n)}(u, v) = 1$ and $F_\varphi^{(n)}(u, v) = 0$, for $n = 1, ..., N$.

- Measurement set-up
  - Type of sampling: uniform sampling in the (u, v) plane;
  - Number of points in the visible range: $K = 1961$;
  - Ratio between measurements and number of elements: $\nu = \frac{K}{N} \simeq 1.0$ $(\nu^{(opt)})$;
- BCS solver
  - Noise variance: $\eta = 5 \times 10^{-1}$ $(\eta^{(opt)})$;
  - Tolerance factor: $\iota = 10^{-8}$;
- Signal-to-Noise-Ratio: $SNR = \{10; 20; ...; 100\}$.

Results

$\Phi = \frac{N_f}{N} = 1\%$ $(N_f = 20)$ - **Best and Worst** BCS **Reconstructions**

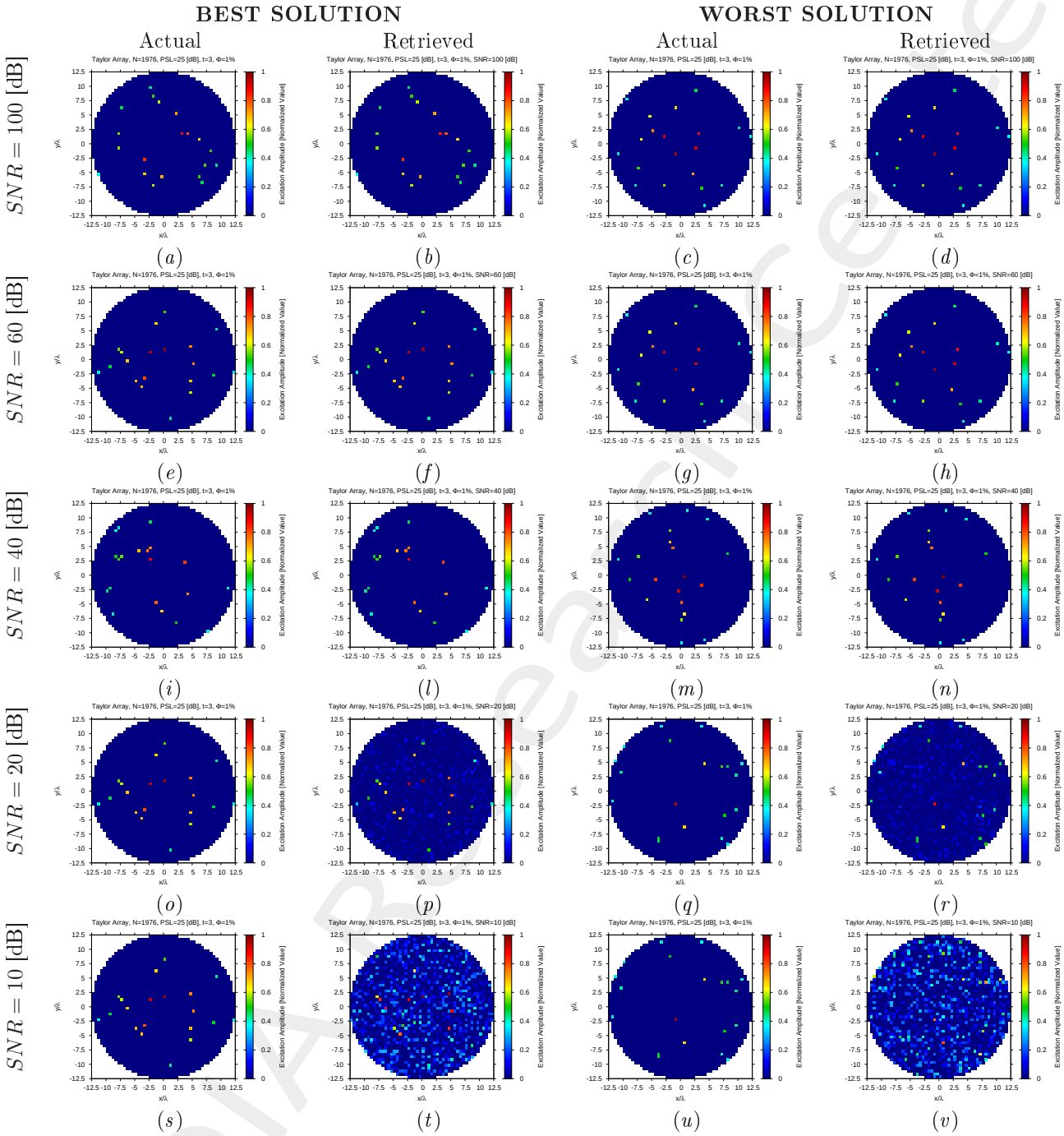

Figure 18: Taylor Array ($N = 1976$, $PSL = 25$ [dB], $t = 3$, $\Phi = 1\%$) - Best and worst reconstructions by BCS under several SNR values.

$\Phi = \frac{N_f}{N} = 2\%$ $(N_f = 40)$ - **Best and Worst** BCS **Reconstructions**

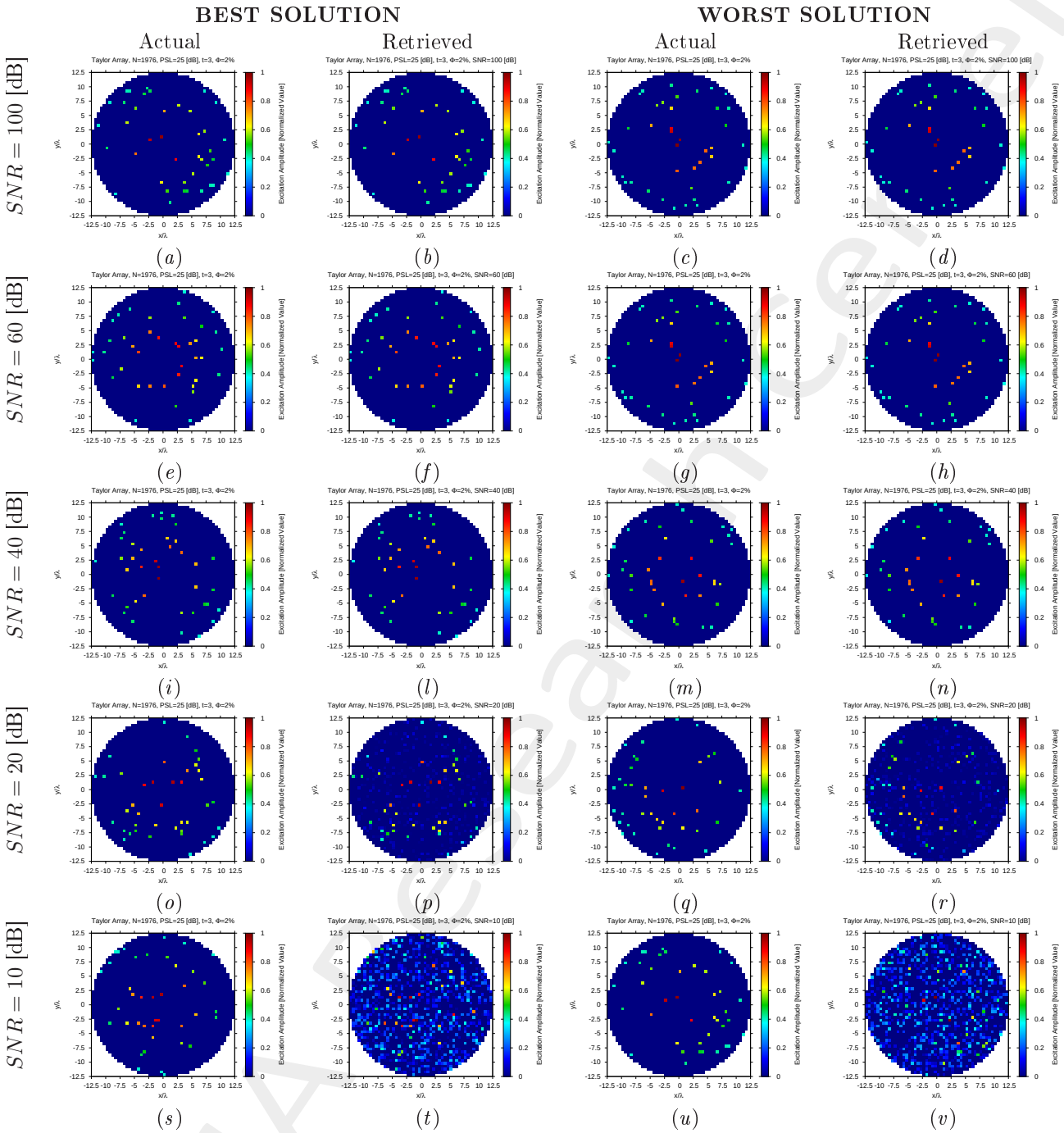

Figure 19: Taylor Array ($N = 1976$, $PSL = 25$ [dB], $t = 3$, $\Phi = 2\%$) - Best and worst reconstructions by BCS under several SNR values.

$\Phi = \frac{N_f}{N} = 4\%$ ($N_f = 79$) - **Best and Worst** BCS **Reconstructions**

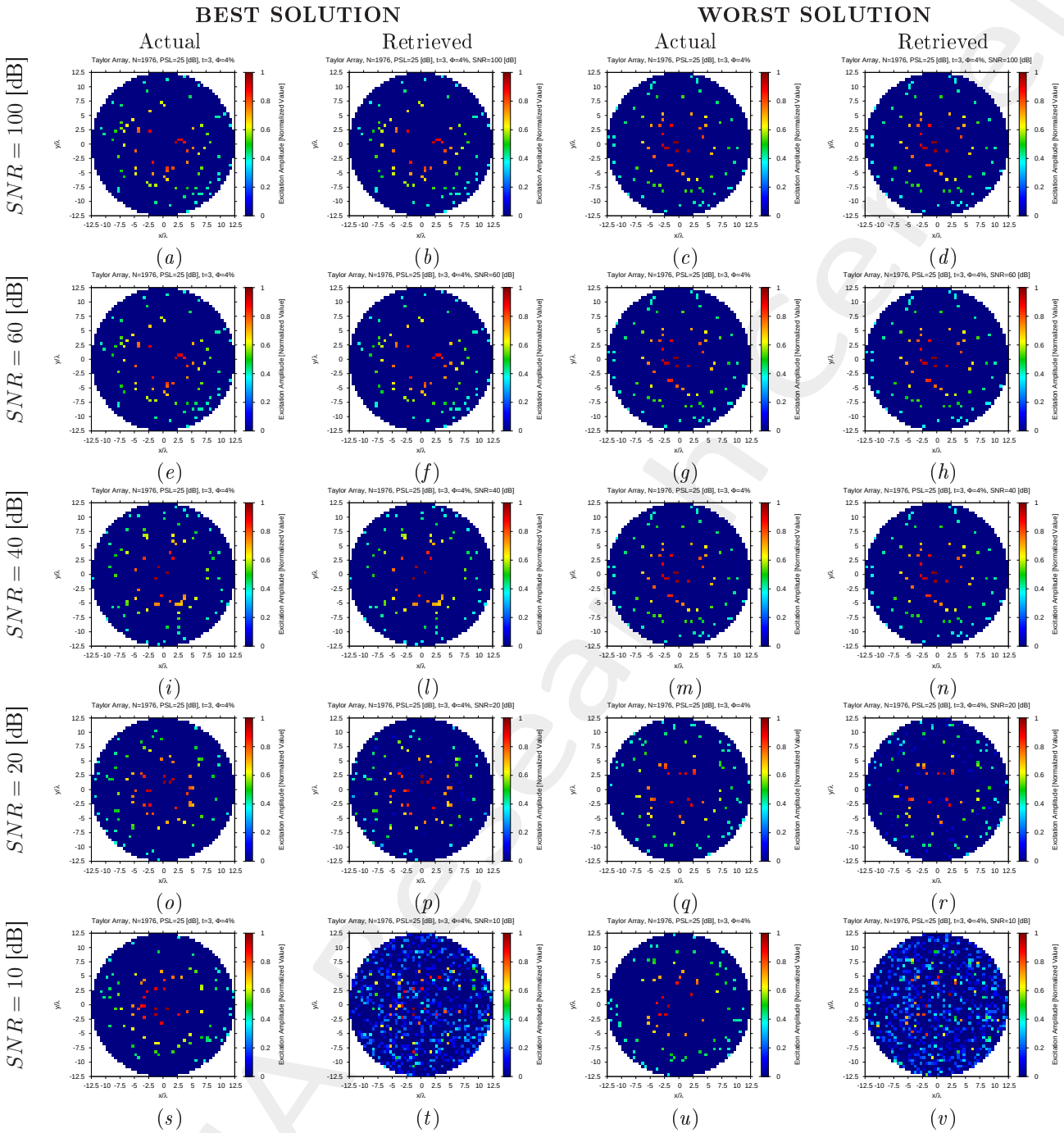

Figure 20: Taylor Array ($N = 1976$, $PSL = 25$ [dB], $t = 3$, $\Phi = 4\%$) - Best and worst reconstructions by BCS under several SNR values.

$\Phi = \frac{N_f}{N} = 8\%$ $(N_f = 158)$ - **Best and Worst** BCS **Reconstructions**

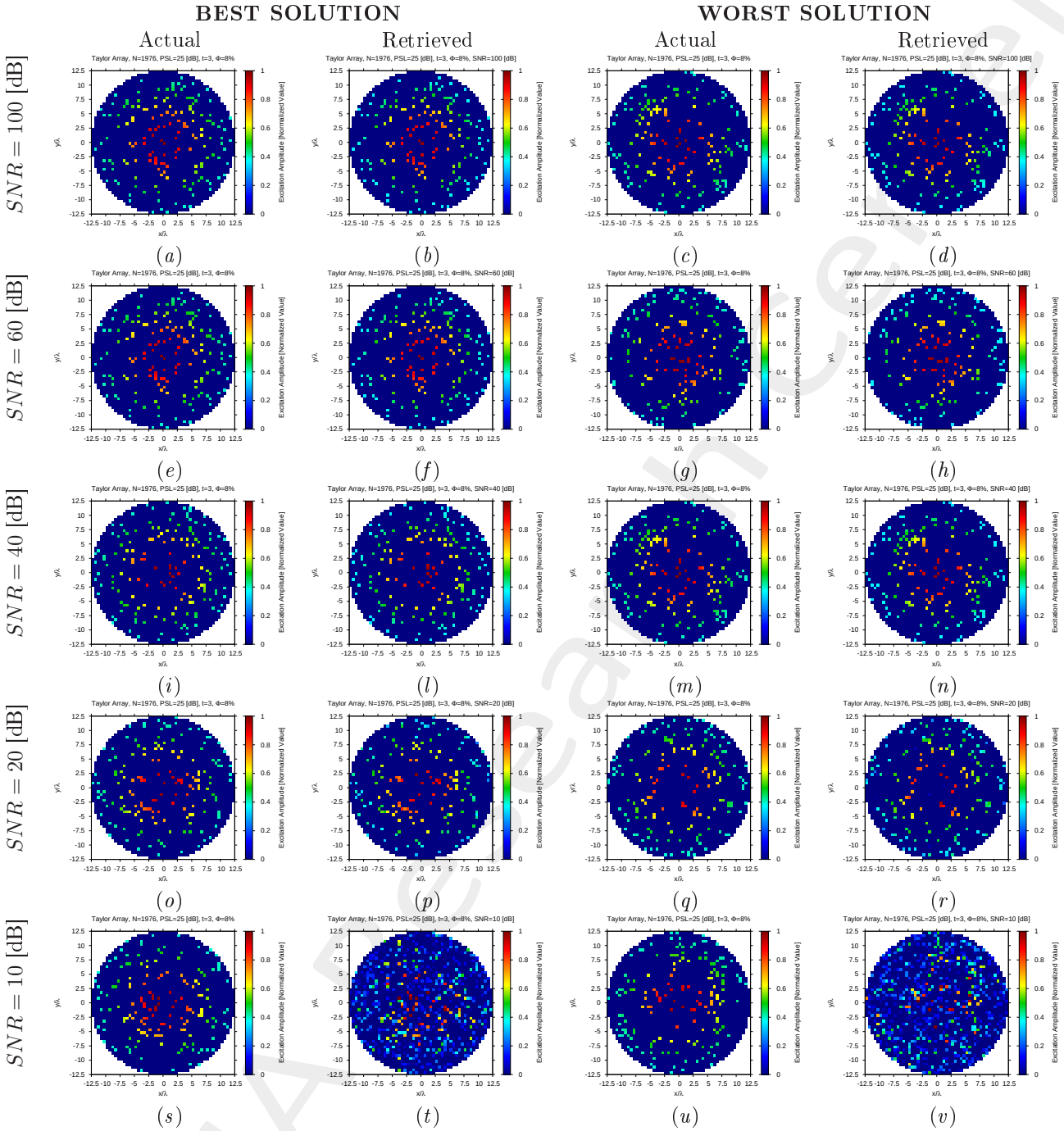

Figure 21: Taylor Array ($N = 1976$, $PSL = 25$ [dB], $t = 3$, $\Phi = 8\%$) - Best and worst reconstructions by BCS under several SNR values.

$\Phi = \frac{N_f}{N} = 16\%$ $(N_f = 316)$ - **Best and Worst** BCS **Reconstructions**

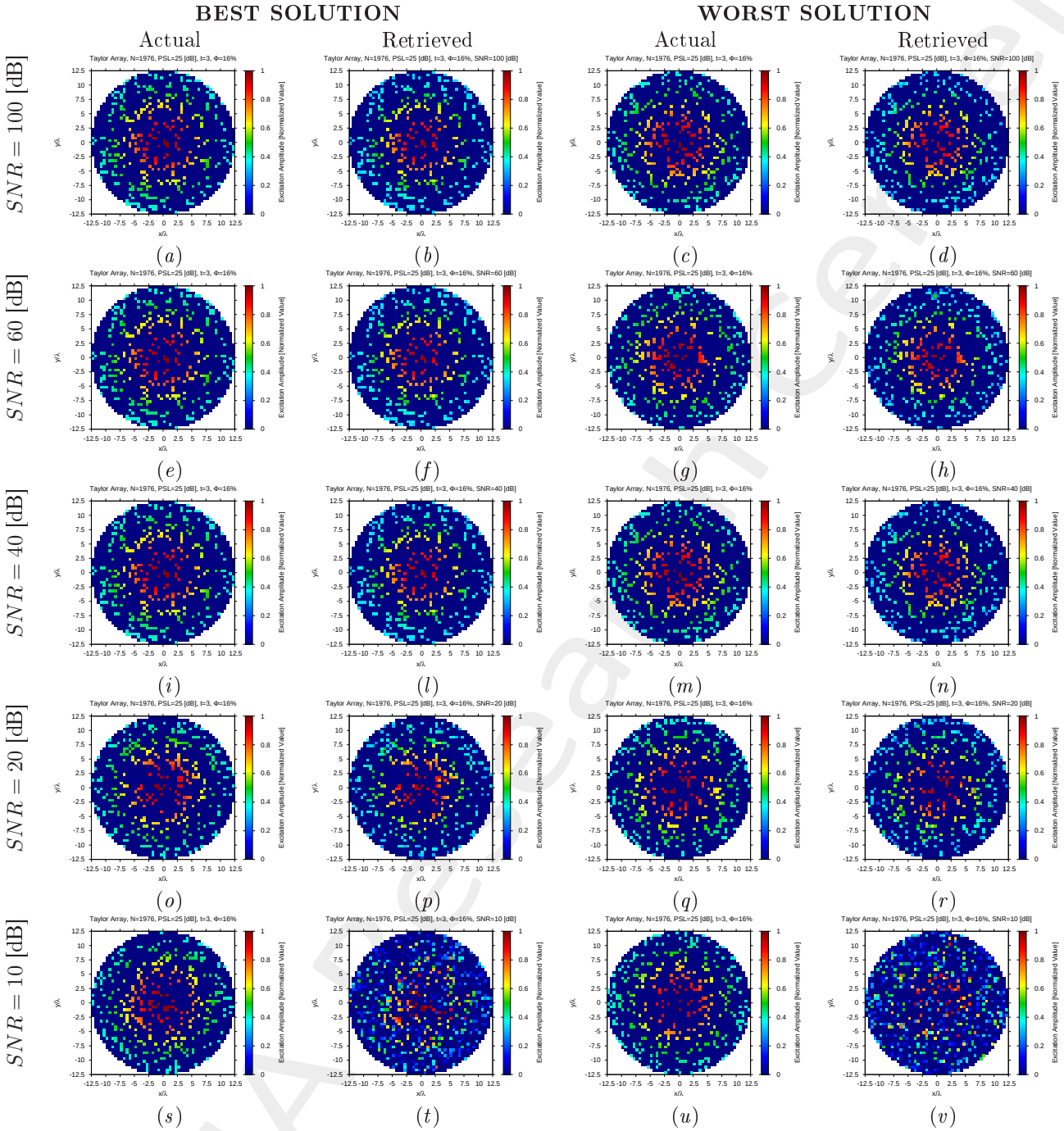

Figure 22: Taylor Array ($N = 1976$, $PSL = 25$ [dB], $t = 3$, $\Phi = 16\%$) - Best and worst reconstructions by BCS under several SNR values.

Diagnosis Error and Confidence Level

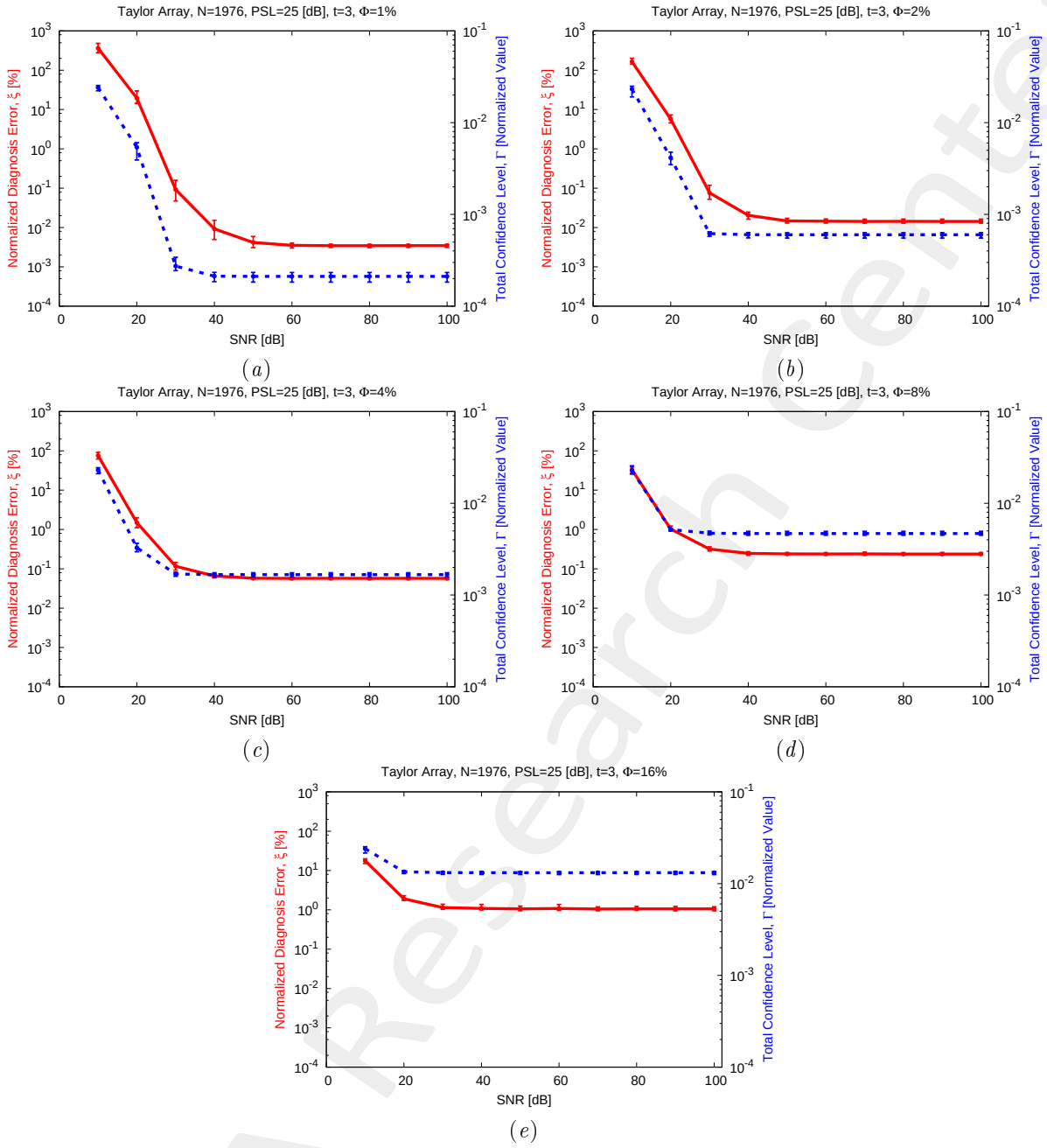

Figure 23: Taylor Array ($N = 1976$, $PSL = 25$ [dB], $t = 3$) - Behavior of the average, minimum and maximum diagnosis error (ξ) and total confidence level (Γ) versus the SNR, for (a) $\Phi = 1\%$, (b) $\Phi = 2\%$, (c) $\Phi = 4\%$, (d) $\Phi = 8\%$, and (e) $\Phi = 16\%$.

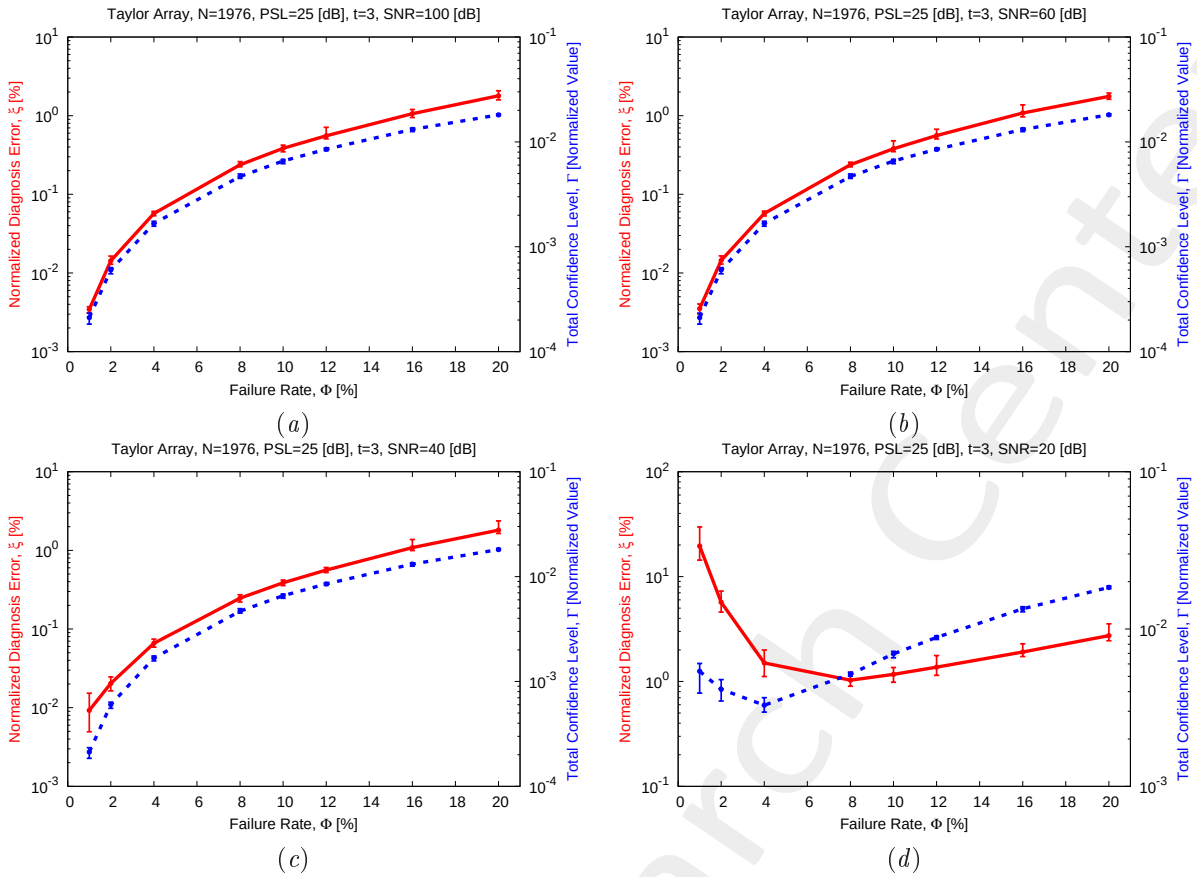

Figure 24: Taylor Array ($N = 1976$, $PSL = 25$ [dB], $t = 3$) - Behavior of the average, minimum and maximum diagnosis error (ξ) and total confidence level (Γ) versus the failure rate (Φ), for (a) $SNR = 100$ [dB], (b) $SNR = 60$ [dB], (c) $SNR = 40$ [dB], and (d) $SNR = 20$ [dB].

1.4 Taylor Array, Analysis vs. Array Size (N)

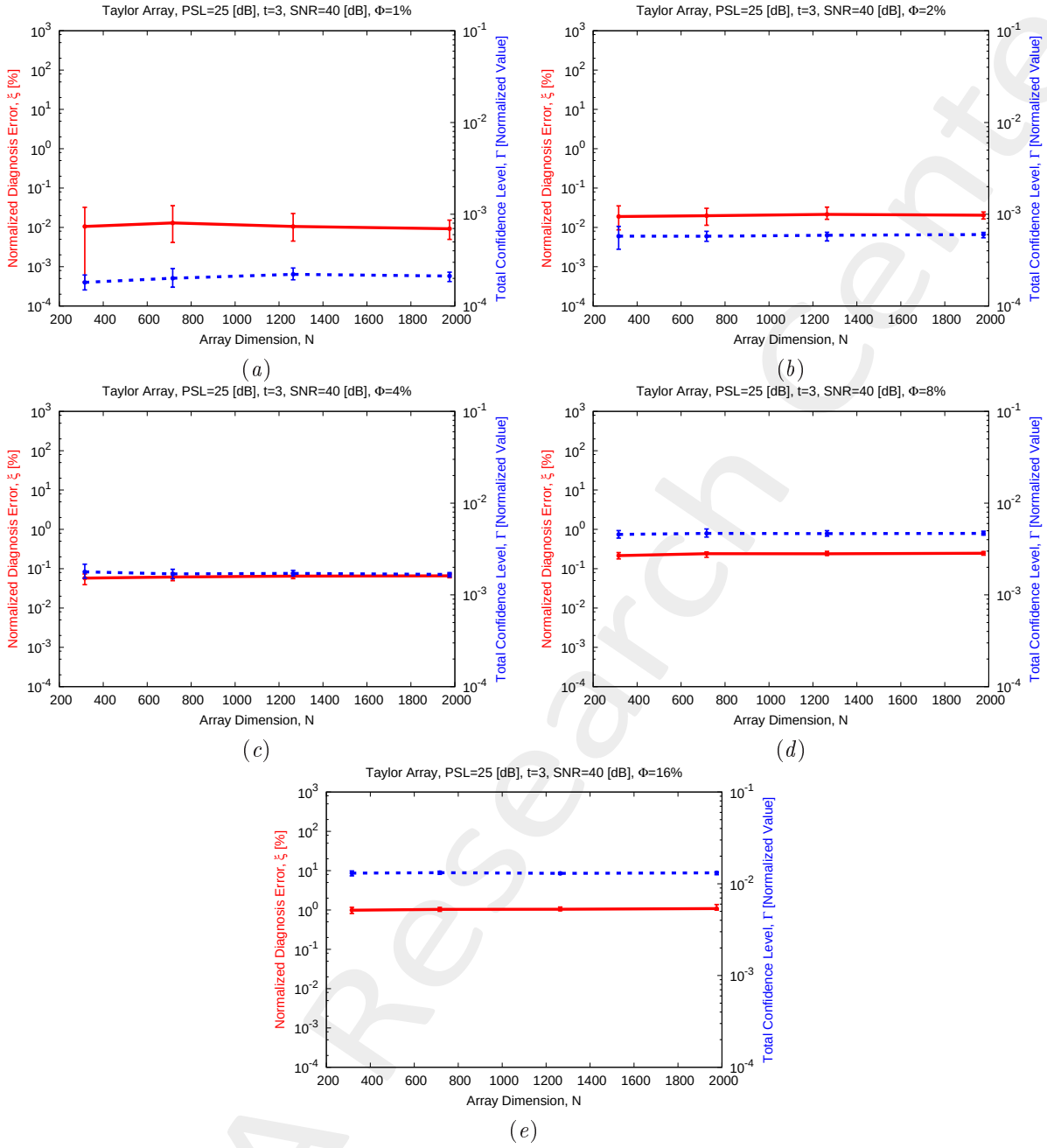

Figure 25: Taylor Array ($PSL = 25$ [dB], $t = 3$), $SNR = 40$ [dB] - Behavior of the average, minimum and maximum diagnosis error (ξ) and total confidence level (Γ) versus the array dimension (N), for (a) $\Phi = 1\%$, (b) $\Phi = 2\%$, (c) $\Phi = 4\%$, (d) $\Phi = 8\%$, and (e) $\Phi = 16\%$.

More information on the topics of this document can be found in the following list of references.

References

[1] P. Rocca, G. Oliveri, R. J. Mailloux, and A. Massa, "Unconventional phased array architectures and design methodologies - A Review," *Proc. IEEE*, vol. 104, no. 3, pp. 544-560, Mar. 2016.

[2] G. Oliveri, G. Gottardi, F. Robol, A. Polo, L. Poli, M. Salucci, M. Chuan, C. Massagrande, P. Vinetti, M. Mattivi, R. Lombardi, and A. Massa, "Co-design of unconventional array architectures and antenna elements for 5G base stations," *IEEE Trans. Antennas Propag.*, vol. 65, no. 12, pp. 6752-6767, Dec. 2017.

[3] G. Oliveri, P. Rocca, and A. Massa, "Reliable diagnosis of large linear arrays - a Bayesian compressive sensing approach," *IEEE Trans. Antennas Propag.*, vol. 60, no. 10, pp. 4627-4636, Oct. 2012.

[4] M. Salucci, A. Gelmini, G. Oliveri, and A. Massa, "Planar arrays diagnosis by means of an advanced Bayesian compressive processing," *IEEE Trans. Antennas Propag.*, vol. 66, no. 11, pp. 5892-5906, Nov. 2018.

[5] A. Massa, P. Rocca, and G. Oliveri, "Compressive sensing in electromagnetics - A review," *IEEE Antennas Propag. Mag.*, pp. 224-238, vol. 57, no. 1, Feb. 2015.

[6] G. Oliveri, M. Salucci, N. Anselmi, and A. Massa, "Compressive sensing as applied to inverse problems for imaging: theory, applications, current trends, and open challenges," *IEEE Antennas Propag. Mag.*, vol. 59, no. 5, pp. 34-46, Oct. 2017.

[7] P. Rocca, M. A. Hannan, M. Salucci, and A. Massa, "Single-snapshot DoA estimation in array antennas with mutual coupling through a multi-scaling Bayesian compressive sensing strategy," *IEEE Trans. Antennas Propag.*, vol. 65, no. 6, pp. 3203-3213, Jun. 2017.

[8] M. Carlin, P. Rocca, G. Oliveri, F. Viani, and A. Massa, "Directions-of-arrival estimation through Bayesian Compressive Sensing strategies," *IEEE Trans. Antennas Propag.*, vol. 61, no. 7, pp. 3828-3838, Jul. 2013.

[9] L. Poli, G. Oliveri, P. Rocca, M. Salucci, and A. Massa, "Long-distance WPT unconventional arrays synthesis," *J. Electromagn. Waves Appl.*, vol. 31, no. 14, pp. 1399-1420, Jul. 2017.

[10] G. Oliveri, M. Salucci, and A. Massa, "Synthesis of modular contiguously clustered linear arrays through a sparseness-regularized solver," *IEEE Trans. Antennas Propag.*, vol. 64, no. 10, pp. 4277-4287, Oct. 2016.

[11] G. Oliveri and A. Massa, "Bayesian compressive sampling for pattern synthesis with maximally sparse non-uniform linear arrays," *IEEE Trans. Antennas Propag.*, vol. 59, no. 2, pp. 467-481, Feb. 2011.

[12] N. Anselmi, G. Oliveri, M. A. Hannan, M. Salucci, and A. Massa, "Color compressive sensing imaging of arbitrary-shaped scatterers," *IEEE Trans. Microw. Theory Techn.*, vol. 65, no. 6, pp. 1986-1999, Jun. 2017.

[13] N. Anselmi, G. Oliveri, M. Salucci, and A. Massa, "Wavelet-based compressive imaging of sparse targets," *IEEE Trans. Antennas Propag.*, vol. 63, no. 11, pp. 4889-4900, Nov. 2015.

[14] L. Poli, G. Oliveri, F. Viani, and A. Massa, “MT-BCS-based microwave imaging approach through minimum-norm current expansion," *IEEE Trans. Antennas Propag.*, vol. 61, no. 9, pp. 4722-4732, Sep. 2013.

[15] G. Oliveri, N. Anselmi, and A. Massa, “Compressive sensing imaging of non-sparse 2D scatterers by a total-variation approach within the Born approximation," *IEEE Trans. Antennas Propag.*, vol. 62, no. 10, pp. 5157-5170, Oct. 2014.

[16] L. Poli, G. Oliveri, and A. Massa, “Imaging sparse metallic cylinders through a local shape function bayesian compressive sensing approach," *J. Opt. Soc. Am. A*, vol. 30, no. 6, pp. 1261-1272, 2013.

[17] L. Poli, G. Oliveri, P. Rocca, and A. Massa, “Bayesian compressive sensing approaches for the reconstruction of two-dimensional sparse scatterers under TE illumination," *IEEE Trans. Geosci. Remote Sens.*, vol. 51, no. 5, pp. 2920-2936, May 2013.

[18] L. Poli, G. Oliveri, and A. Massa, “Microwave imaging within the first-order Born approximation by means of the contrast-field Bayesian compressive sensing," *IEEE Trans. Antennas Propag.*, vol. 60, no. 6, pp. 2865-2879, Jun. 2012.

[19] G. Oliveri, L. Poli, P. Rocca, and A. Massa, “Bayesian compressive optical imaging within the Rytov approximation," *Opt. Lett.*, vol. 37, no. 10, pp. 1760-1762, 2012.

[20] G. Oliveri, P. Rocca, and A. Massa, “A Bayesian compressive sampling-based inversion for imaging sparse scatterers," *IEEE Trans. Geosci. Remote Sens.*, vol. 49, no. 10, pp. 3993-4006, Oct. 2011.

[21] N. Anselmi, L. Poli, G. Oliveri, and A. Massa, “Iterative multi-resolution bayesian CS for microwave imaging," *IEEE Trans. Antennas Propag.*, vol. 66, no. 7, pp. 3665-3677, Jul. 2018.

[22] L. Poli, P. Rocca, G. Oliveri, and A. Massa, “Failure correction in time-modulated linear arrays," *IET Radar, Sonar & Navigation*, vol. 8, no. 3, pp. 195-201, 2014.